Citation for published version:
Najafi, HR, Robinson, F, Dastyar, F & Samadi, AA 2009, Small-disturbance voltage stability of distribution systems with wind turbine implemented with WRIG. in International Conference on Power Engineering, Energy and Electrical Drives. POWERENG '09. IEEE, Lisbon, Portugal, pp. 191 - 195.
https://doi.org/10.1109/POWERENG.2009.4915163

DOI:
10.1109/POWERENG.2009.4915163

Publication date:
2009

Document Version
Peer reviewed version

Small-Disturbance Voltage Stability of Distribution Systems with Wind Turbine implemented with WRIG

H.R. Najafi(1) , F.V.P. Robinson(2) , F. Dastyar(1) , A.A. Samadi(1)
(1)University of Birjand, IRAN, (2) University of Bath, U.K
h.r.najafi@birjand.ac.ir, f.dastyar@birjand.ac.ir, a.a.samadi@birjand.ac.ir, f.v.p.robinson@bath.ac.uk

***Abstract*- The small-disturbance voltage stability of a grid-connected wound-rotor induction-generator (WRIG) wind-turbine system is analyzed under different operating conditions. This theoretical study shows the effect of the wound-rotor induction generator and its parameters on load-bus voltage collapse phenomena. Results show that the rotor resistance of the induction generators may decrease the system voltage stability margin and that the transmission line length has an important effect on the maximum loading point and critical point of loading.**

I. INTRODUCTION

In many countries wind power generation is expanding, and satisfying a steadily increasing proportion of national power demand. It has been estimated that the total operating wind-power capacity in the world increased from approximately 2000 MW in 1990 to well over 16,000 MW at the end of 2000. Continued rapid growth is expected, with a predicted 50,000 MW of operating wind-power capacity by 2010 [1].

The impact of induction generators on the short-term or large disturbance voltage stability of distribution systems has been investigated in many papers and is relatively well documented [2-5]. It is understood that during faults, induction generators may accelerate to a high speed, draw a large reactive power from the system and result in voltage collapse [2]. However, much less attention has been paid to the small-disturbance voltage stability of distribution systems connected to induction generators. As more and more induction generators are connected, it is essential to understand the impact of these generators on different distribution system operation-related issues. The importance of this is illustrated here by presenting a theoretical investigation into the influence of induction generators on the small-disturbance voltage stability of distribution systems. The system stability margin is analyzed through the *P-V* curves [6].

In this paper, section II describes the models used to represent the main networks components and the wind turbine; the results of the theoretical analysis are explained in section III; and the conclusions of the work are summarized in Section IV.

II. SYSTEM COMPONENTS AND MODELING

A. Wind-energy conversion system model

The basic model of the conversion system is shown in Figure 1. P_w, the wind power, is converted by the turbine at angular velocity, ω_m, to mechanical power, P_m, which is then supplied to the mechanical-transmission system. The mechanical-transmission output power, P_t, is reduced by the imperfect transmission efficiency η_m as shown in (1).

$$p_t = \eta_m \times p_m \tag{1}$$

The generator output power P_e is reduced by the imperfect generation efficiency η_g as shown in (2).

$$p_e = \eta_g \times p_t \tag{2}$$

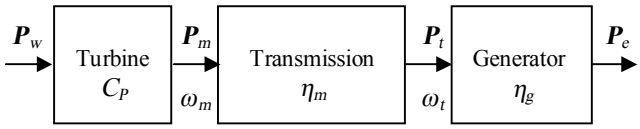

Fig. 1. Wind-turbine electrical system.

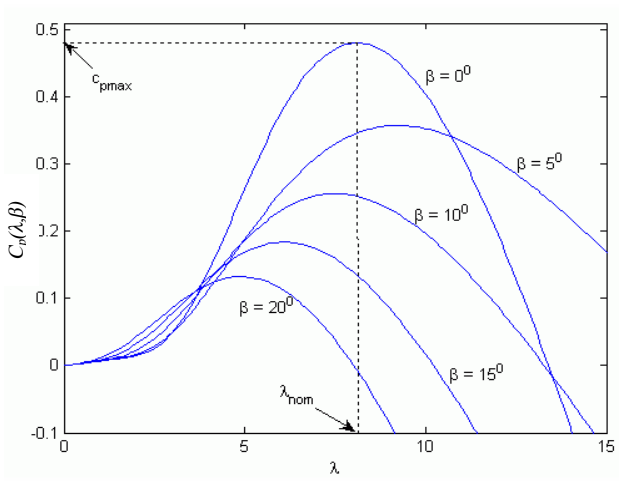

Fig. 2. Constant β performance $C_P(\lambda,\beta)$ characteristics for wind turbine.

Equations (1) and (2) combine to relate electrical power output to wind power input as shown in (3).

$$p_e = \eta_m \times \eta_g \times c_p \times p_w \tag{3}$$

Term η_g is the generator efficiency, C_p is the wind-turbine performance coefficient and p_w is the wind power that is obtained using (4) as in [7].

$$p_w = \frac{1}{2}\rho\ A V_w^{\ 3} \tag{4}$$

$$p_m = \frac{1}{2}\rho\ C_p(\lambda,\beta)\ A V_w^{\ 3} \tag{5}$$

Term ρ is the air density, A is the area swept by wind turbine blades, $\lambda = R\Omega_b / V_w$ is the ratio of blade tip speed to wind speed, Ω_b is the wind turbine rotational speed (rad/sec), and V_w is the wind speed. The wind-turbine blade aerodynamic performance is characterized by a non- dimensional curve of torque coefficient C_P as a function of tip-speed ratio λ for various blade-pitch angle, β, values. $C_P(\lambda,\beta)$ is evaluated from (6) and (7) using the following representative values for the coefficients: c_1 = 0.5176, c_2 = 116, c_3 = 0.4, c_5 = 21, c_6 = 0.0068.

$$C_p(\lambda,\beta) = c_1\left(\frac{c_2}{\lambda_i} - c_3\beta - c_4\right)e^{\frac{-c_5}{\lambda_i}} + c_6\lambda \tag{6}$$

$$\frac{1}{\lambda_i} = \frac{1}{\lambda + 0.08\beta} - \frac{0.035}{\beta^3 + 1} \tag{7}$$

A family of constant blade-pitch-angle performance curves for a typical wind turbine is shown in figure 2 [8-9].

B. Wound rotor induction generator

The equivalent circuit of an induction generator is shown in figure 3.

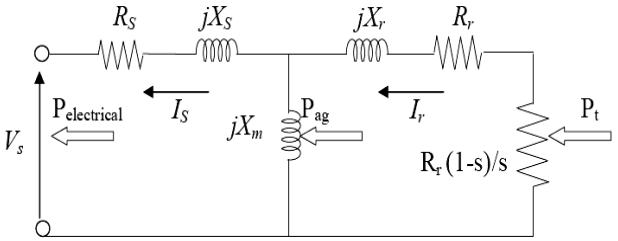

Fig. 3. Equivalent circuit of induction generator

Using this model, equations (8) to (10) give Thevenin equivalent circuit values [6].

$$Z_{TH} = R_S + jX_S + (jX_m \| (R_r/s + jX_r)) \tag{8}$$

$$|I_S| = \frac{\sqrt{(R_r/s)^2 + (X_m + X_r)^2}}{X_m} \times \sqrt{\frac{p_t}{3R_r\left(\frac{1-s}{s}\right)}} \quad \angle\theta_z^{\ 0} \tag{9}$$

$$V_S = |Z_{TH}|\,|I_S|\ \angle 0^0 \tag{10}$$

Power P_t is the mechanical-transmission output which, if friction is neglected, approximates to the input power delivered to the equivalent circuit (shaft mechanical power per phase) as given by (11).

$$p_t = R_r\left(\frac{1-s}{s}\right)I_r^{\ 2} \tag{11}$$

The electric power output per phase is therefore given by (12).

$$p_e = R_r\left(\frac{1}{s}\right)I_r^{\ 2} + \underbrace{R_S\ I_S^{\ 2}}_{\substack{STATOR\\ LOSS}} \tag{12}$$

The plus sign in the above equation arises because of the negative slip of the generating induction machine which leads to generated power being negative. Terms R_S, R_r, X_s, X_m, X_r correspond to stator and rotor resistances, and stator magnetizing and rotor reactances respectively. Also s is slip.

C. System under study

Figure 4 shows a single-line diagram of the system used to investigate stability. The wind farm is connected to an electrical network through a 25 kV transmission line and ideal transformer with n1:n2 turns ratio. The transmission line is represented by a π-model with **A**, **B**, **C** and **D** parameters discussed later and a load, P + jQ, is located at wind-farm bus. Transmission-line and wound-rotor induction-generator parameters are presented in the Appendix. Wind turbine parameters are taken from [8].

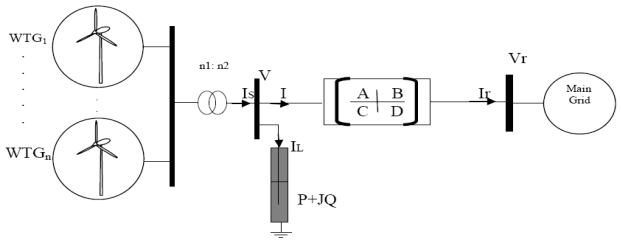

Fig. 4. Single-line diagram of wind farm connection to main grid.

III. RESULTS

To evaluate the small-disturbance voltage stability of the figure 4 induction-generator wind-farm under different conditions, the lossless transmission-line relationships and parameters used are given by (13). The results of the theoretical modeling of performance will now be presented and interpreted in the following sub-sections.

$$\begin{pmatrix} V \\ I \end{pmatrix} = \begin{pmatrix} \cos(\beta l) & j z_c \sin(\beta l) \\ j\sin(\beta l)/z_c & \cos(\beta l) \end{pmatrix} \begin{pmatrix} V_r \\ I_r \end{pmatrix} \tag{13}$$

$$\beta = \omega\sqrt{LC}\ ,\ z_c = \sqrt{\frac{L}{C}}$$

Variables V, I, V_r, I_r are identified in figure 4, l, z_c, β, L, C and ω are transmission-line length, characteristic impedance, phase constant line inductance per kilometer, line capacitance per kilometer and angular frequency, respectively.

A. P-V curve at wind farm bus of system under study

To evaluate the effect of the wind farm's wound-rotor induction generators on the maximum loading point or critical load power, the *P-V* curve for the load bus must be investigated for operation with and without the wind turbine. To start the KCL equation at load bus is developed as below.

$$i = i_s - i_L \tag{14}$$

$$i_L = \frac{P - jQ}{v^*} \tag{15}$$

$$v = v_r \cos(\beta l) + j z_c \sin(\beta l)\, i_r \tag{16}$$

Substituting i_r from (13) into (16) gives (17).

$$v = v_r \cos(\beta l) + j z_c \tan(\beta l)\,(i - \frac{j \sin(\beta l)}{z_c} v_r) = \tag{17}$$
$$v_r \cos(\beta l) + j z_c \tan(\beta l) i + \tan(\beta l) \sin(\beta l) v_r$$

Substituting i and i_L from (14) and (15) into (17) gives (18).

$$v = v_r \cos(\beta l) + j z_c \tan(\beta l)\,(i_s - \frac{P_L - jQ_L}{v^*}) + \tan(\beta l) \sin(\beta l) v_r \tag{18}$$

In (18), i_s is the total wind-farm current. Setting the real and imaginary part of (18) to zero gives (19).

$$v^2 + v\left[z_c \tan(\beta l) \sin(\varphi) i_s - v_r\left(\cos(\beta l) + \sin(\beta l) \tan(\beta l)\right)\right] + P_L z_c \tan(\varphi_L) \tan(\beta l) = 0 \tag{19}$$

The roots of (19) are given in (20).

$$v = \frac{-\left[z_c \tan(\beta l) \sin(\varphi) i_s - v_r\left(\cos(\beta l) + \sin(\beta l) \tan(\beta l)\right)\right]}{2} \pm \ldots\ldots \tag{20}$$
$$\ldots \frac{\sqrt{\left[z_c \tan(\beta l) \sin(\varphi) i_s - v_r\left(\cos(\beta l) + \sin(\beta l) \tan(\beta l)\right)\right]^2 - 4 P_L z_c \tan(\varphi_L) \tan(\beta l)}}{2}$$

Thus the critical loading values are given by equations (21) and (22).

$$p_{L\,critical} = \frac{\left[z_c \tan(\beta l) \sin(\varphi) i_s - v_r\left(\cos(\beta l) + \sin(\beta l) \tan(\beta l)\right)\right]^2}{4 z_c \tan(\varphi_L) \tan(\beta l)} \tag{21}$$

$$Q_{L\,critical} = \frac{\left[z_c \tan(\beta l) \sin(\varphi) i_s - v_r\left(\cos(\beta l) + \sin(\beta l) \tan(\beta l)\right)\right]^2}{4 z_c \tan(\beta l)} \tag{22}$$

From (21) and (22) it is apparent that the active power of critical loading varies with φ_L but the reactive power is fixed. Figure 7 shows the per-phase *P-V* curve at the wind-turbine load bus for different input mechanical power. This result shows that the different input mechanical power does not have a detrimental effect on the voltage collapse diagram.

The effect of various forms of input mechanical power was examined; first with the wind farm performing as one 10 MW turbine and then performing as ten 1MW turbines. In both, the total mechanical power is equal. Figure 8 gives the resulting *P-V* curves and shows that the different form of input mechanical power has a weak effect on the voltage collapse diagram.

Figure 9 gives the rotor-resistance effect on critical-loading power at the wind-farm bus and shows that critical loading power varies with changing rotor resistance. This curve shows the existence of a minimum critical-loading power. Descending or ascending from this point causes critical-loading-power increase. However, rotor losses must also be considered.

One of the important parameters in voltage-collapse phenomena in power systems is line length. Figure 10 shows the transmission line-length effect on critical loading power at the wind-farm bus. It is obvious that with increasing line-length critical-loading power decreases.

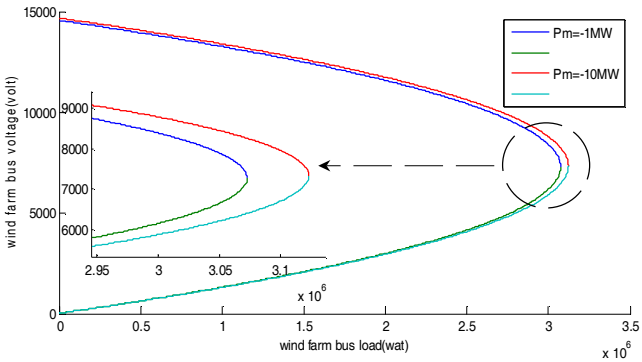

Fig. 7. Per phase *P-V* curve for different input mechanical power.

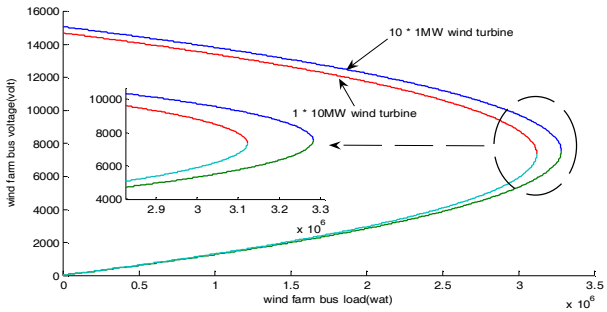

Fig. 8. *P-V* curve for different forms of mechanical power.

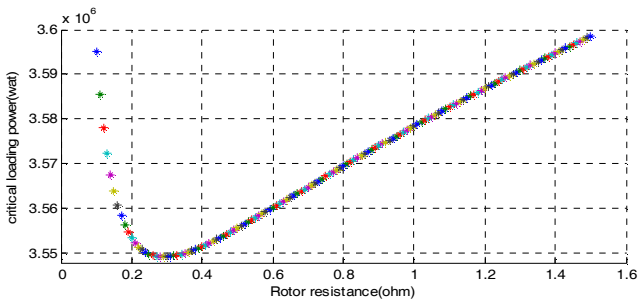

Fig. 9. Rotor resistance effect on critical loading power.

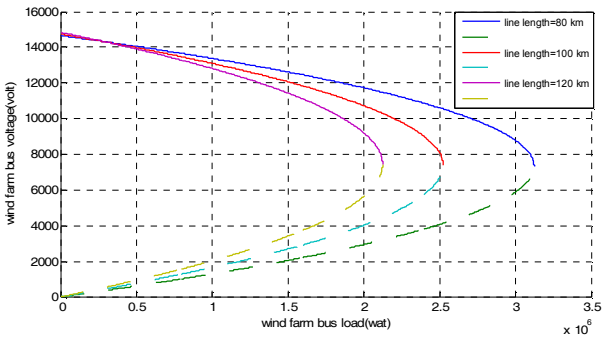

Fig. 10. The effect of transmission-line length on critical loading power.

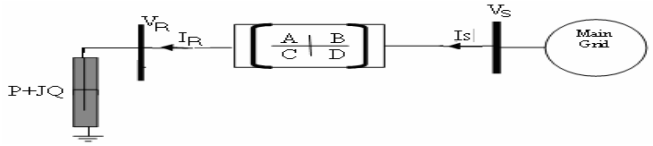

Fig. 11. Main grid with no wind-farm connection.

The maximum loading point or critical load power for the main grid without the wind-farm connection is now examined using figure 11. A similar analysis to that just used with a wind-farm connection is repeated, giving equations (23) to (27).

$$I_R = \frac{P - jQ}{V_R^*} \tag{23}$$

$$V_S = V_R Cos(\beta l) + jz_c Sin(\beta l)\frac{p - jQ}{V_R^*} = V_R Cos\ \theta + jz_c Sin(\beta l)\frac{p - j\,p\tan\varphi}{V_R} \tag{24}$$

$$V_R^* V_S = |V_R|^2 \cos(\beta l) + jz_c \sin(\beta l)\, p + ... \quad .....z_c \sin(\beta l)\, p\tan\varphi \tag{25}$$

$$V_R^{\,4}\cos^2(\beta l) + V_R^{\,2}(z_c\ p\tan(\varphi)\sin(2\beta l) - V_s^{\,2}).... \quad .... + \frac{z_c^{\,2}\sin^2(\beta l)\, p^2}{\cos^2(\varphi)} = 0 \tag{26}$$

The critical loading value is given by (27).

$$p_{L\,critical} = \frac{V_S^{\,2}(1 - \sin(\varphi))}{z_c \cos(\varphi)\sin(2\beta l)} \tag{27}$$

Figure 12 illustrates the effect of the wound-rotor induction generator on the voltage-collapse characteristic of the main grid. It shows that the induction generator has an important effect on the voltage collapse diagram: the critical loading power is improved.

The effect of a shunt compensator located at load bus is also examined using a similar analysis; see Figure 13 and equations (28) to (31). The corresponding *P-V* results are given in Figure 14.

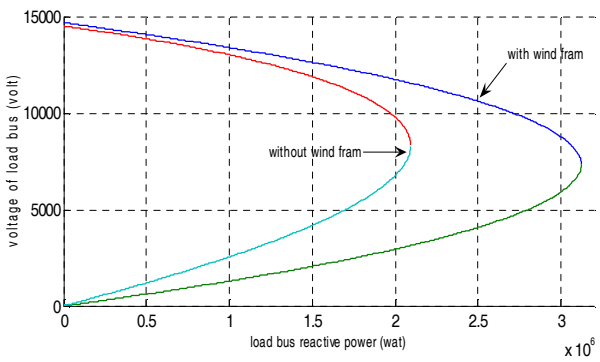

Fig. 12. Effect of induction generators on voltage collapse characteristics.

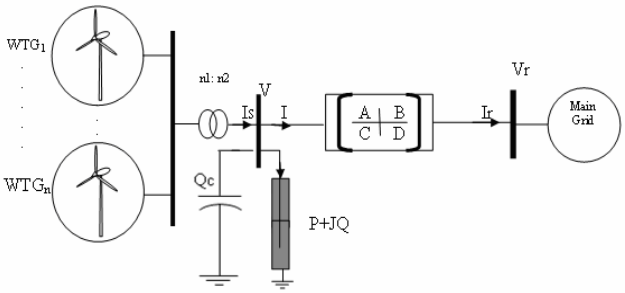

Fig. 13. Power system with shunt compensator.

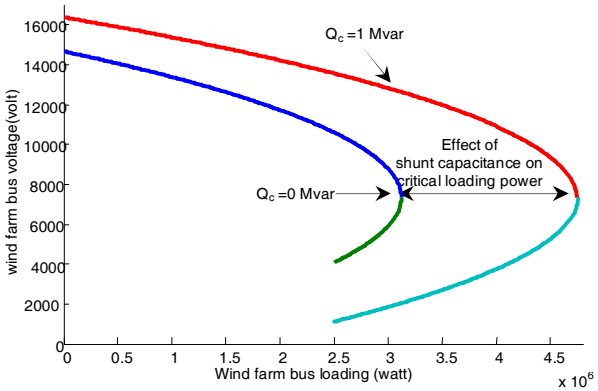

Fig. 14. Effect of shunt compensator on voltage collapse characteristics.

$$i = i_s - \frac{P - j(Q - Q_C)}{v^*} \tag{28}$$

$$v^2 + v\left[z_c \tan(\beta l)\sin(\varphi) i_s - v_r(\cos(\beta l) + \sin(\beta l)\tan(\beta l))\right] + ... \quad ....P_L z_c \tan(\varphi_L)\tan(\beta l) - z_c Q_c \tan(\beta l) = 0 \tag{29}$$

$$v = \frac{-[z_c \tan(\beta l)\sin(\varphi) i_s - v_r(\cos(\beta l) + \sin(\beta l)\tan(\beta l))]}{2} \pm \left[\frac{\sqrt{[z_c \tan(\beta l)\sin(\varphi) i_s - v_r(\cos(\beta l) + \sin(\beta l)\tan(\beta l))]^2 .....}}{2} \right. \left. \frac{\sqrt{..... - 4(P_L z_c \tan(\varphi_L)\tan(\beta l) - z_c Q_c \tan(\beta l))}}{2}\right] \tag{30}$$

The critical loading value is given by (31).

$$p_{L\,critical} = \frac{[z_c \tan(\beta l)\sin(\varphi) i_s - v_r(\cos(\beta l) + \sin(\beta l)\tan(\beta l))]^2}{4 z_c \tan(\varphi_L)\tan(\beta l)} + \frac{Q_c}{\tan(\varphi_L)} \tag{31}$$

The difference between the critical loading power with and without the shunt compensator is obtained using (32).

$$\Delta p_{L\,critical} = \frac{Q_C}{\tan(\beta l)} \tag{32}$$

Equation (32) shows that this difference depends on several factors; namely, reactive power injected by the shunt capacitance, phase constant of line and line length. Figure 14 shows the effect of the load-bus shunt compensator on the voltage collapse characteristic.

IV. CONCLUSIONS

A theoretical investigation into the impact of wound rotor induction generators on the long-term or small-disturbance voltage stability of distribution systems has been presented. Analytical results show that the rotor resistance influence on voltage collapse phenomena is varied. Line-length and shunt capacitance effects were investigated. With increasing line length, critical-loading power decreases. A shunt compensator was connected to the wind-turbine load bus and its effect was seen to depend on the reactive power injected by shunt capacitance, the phase constant of the line and its length. The wound-rotor induction generator was shown to have an important effect on the voltage collapse diagram and gave an improvement in critical loading power.

APPENDIX

TABLE I

WOUND ROTOR INDUCTION GENERATOR

Parameter	Value
R_s	0.25Ω
Rr	0.2Ω
Xs	0.5Ω
Xr	0.5Ω
X_m	30Ω
P(pole)	4
f(frequency)	60
S(slip)	-0.03

TABLE II

TRANSMISSION LINE PARAMETERS

Z	0.032+j0.35 Ω/km
Y	j4.2 × 10^{-6} S/km

REFERENCES

[1] J.O.G. Tande. Uhlen ,"Wind turbines in weak grids-constraints and solutions", Electricity Distribution, 2001. Part 1: Contributions. CIRED.16thInternational Conference and Exhibition on (IEE Conf. Pub. No.482), vol. 4, 18-21 June 2001.

[2] N. Jenkins, R. Allan, P. Crossley, D. Kirschen e G. Strbac, Embedded generation, 1st ed., The Institute of Electrical Engineers, 2000.

[3] V. Akhmatov, H. Knudsen, A. H. Nielsen, J. K. Pedersen and N. K. Poulsen, "Modeling and transient stability of large wind farms," International Journal of Electrical Power and Energy Systems, vol. 25, pp. 123-144, 2003.

[4] F. P. Mello, J. W. Feltes, L. N. Hannet and J. C. White, "Application of induction generators in power systems," IEEE Transactions on Power Apparatus and Systems, vol. 101, pp. 3385-3393, 1982.

[5] O. Samuelsson and S. Lindahl, "On speed stability," accepted to be published in Letter Section of the IEEE Transactions on Power Systems (PESL-00013-2004).

[6] P.S. Kundur, "Power System Stability and Control", McGraw-Hill, 1994.

[7] Gary L. Johnson," Wind energy systems", Prentice-Hall, January 1994,

[8] H.R. Najafi, F. Robinson, F. Dastyar, A.A. Samadi, "Transient Stability Evaluation of wind farms implemented with induction generators", UPEC 2008, Conference Proceeding, Italy, 2008.

[9] Matlab simulink toolbox.

BIOGRAPHIES

Hamid Reza Najafi received the B. Eng and M. Eng degrees from University of Ferdowsi, Iran in 1981 and 1991, respectively and PhD from IUST, Iran in 2004. He has been a lecturer at Faculty of Engineering, University of Birjand since 1993, and he currently works as an assistant professor in the Electric Power Group, at University of Birjand, Iran. His special fields of interest include: Power System modeling, HVDC and FACTS, reliability of power systems, distributed generation, application of ANN and fuzzy system in power systems.

Francis V P Robinson (M'1988) gained a PhD from Heriot-Watt University, Edinburgh, Scotland. He has been a lecturer at the Department of Electronic and Electrical Engineering, University of Bath since 1990, and is a member of the Electromagnetic, Machines and Drives Group. His teaching and research are primarily related to power electronics and drives. He has previously worked as a power electronics design engineer with Posidata (Dana) LTD, Rutherford Appleton Laboratory, and GEC Small Machines Ltd. Dr Robinson is a chartered engineer in the UK and a member of the IET and IEEE.

Dastyar F. received his B.Eng. in electrical engineering from Guilan university, Rasht, Iran, in 2006. He is currently pursuing his M. Eng degree at Birjand University. His areas of interest include voltage stability and distributed generation.

Samadi A.A. received his B.Eng. in electrical engineering from the University of Birjand, Iran, in 2006. He is currently pursuing his M. Eng degree at Birjand University. His areas of interest include voltage stability, harmonic analysis, power electronic and distributed generation.